J. Fluid Mech. (1998), *vol.* 359, *pp.* 23–47. Printed in the United Kingdom

© 1998 Cambridge University Press

Prandtl–Meyer flows with homogeneous condensation. Part 1. Subcritical flows

By C. F. DELALE[1] AND D. G. CRIGHTON[2]

[1] Department of Mechanical Engineering, Istanbul University, Avcılar 34850, Istanbul *and* TÜBİTAK Research Institute for Basic Sciences, PO Box 6, 81220 Çengelköy, Istanbul, Turkey

[2] Department of Applied Mathematics and Theoretical Physics, University of Cambridge, Silver Street, Cambridge CB3 9EW, UK

(Received 7 May 1997 and in revised form 5 November 1997)

Prandtl–Meyer flows with heat addition from homogeneous condensation not exceeding a critical value (subcritical flows) are investigated by an asymptotic method in the double limit of a large nucleation time followed by a small droplet growth time. The physically distinct condensation zones, with detailed analytical structure, are displayed along streamlines and the flow field in each zone is determined utilizing the asymptotic solution of the rate equation along streamlines. In particular the nucleation wave front, which corresponds to states of maximum nucleation along streamlines, is accurately located independently of the particular condensation model employed. Results obtained using the classical nucleation equation together with the Hertz–Knudsen droplet growth law show, despite qualitative agreement, considerable differences between the nucleation wave fronts and measured onset conditions for the experiments of Smith (1971), because of intersecting characteristics in the heat addition zones. This shows the necessity of including an embedded oblique shock wave in the expansion fan of corner expansion flows for the cases investigated.

1. Introduction

Non-equilibrium condensation in high-speed expansion flows has been investigated theoretically and experimentally for decades because of its importance in science and technology. For the present time the review articles by Wegener (1969), Gyarmathy (1976), and Kotake & Glass (1981) can serve as a comprehensive introduction to the subject. The theory of two-phase flow with non-equilibrium homogeneous condensation was first formulated by Oswatitsch (1942) by combining the nucleation rate equation with a droplet growth law. Most of the earlier efforts concentrated on experimental and numerical investigation of one-dimensional steady nozzle flows (Wegener & Mack 1958; Wegener & Pouring 1964; Hill 1966; Barschdorff 1971). Steady two-dimensional supersonic nozzle flow with homogeneous condensation was first investigated by Bartlmä (1964) and later by Davydov (1971), Tkalenko (1972) and Bratos & Jaeschke (1974) using the numerical method of characteristics. In this case only subcritical flows, i.e. flows where the amount of heat released by condensation does not exceed a critical value, could be treated. Numerical solutions of steady two-dimensional nozzle flows have only recently been carried out by Schnerr (1989) and Schnerr & Dohrmann (1990) for both subcritical and supercritical flows (flows with an embedded shock due to excessive heat addition by condensation) using the finite volume method.

In addition to nozzle flows, condensation phenomena can also be investigated in

https://doi.org/10.1017/S0022112097008379 Published online by Cambridge University Press

non-stationary rarefaction waves in the driver section of a shock tube and in Prandtl–Meyer flows around a sharp corner. Among the investigations in non-stationary rarefaction waves, one can cite the experimental studies of Courtney (1965), Homer (1971), Kawada & Mori (1973), Barschdorff (1975), Kalra (1975) and Peters (1987). The numerical solution to the problem was discussed by Sislian & Glass (1976), using the numerical method of characteristics, and by Smolders, Niessen & Van Dongen (1992) using the random choice method. An asymptotic closed-form solution of the problem has recently been given by Delale, Schnerr & Zierep (1995). Condensation phenomena in supersonic expansion flows around a sharp corner (Prandtl–Meyer flows) have been investigated experimentally and numerically by Smith (1971), Kurshakov, Saltanov & Tkalenko (1971) and Frank (1979, 1985). The experiments mainly concentrated on measurements of the onset conditions, using a Mach–Zehnder interferometer, whereas numerical solutions employed the method of characteristics in the absence of embedded shock waves. None of the numerical and experimental investigations performed to date are sufficient in satisfactorily describing Prandtl–Meyer flows with homogeneous condensation, particularly supercritical flows, and further investigations need to be pursued (for example, a finite volume computation of these flows should prove to be useful).

It is the aim of this investigation to analyse these flows by an asymptotic method which was originally given by Blythe & Shih (1976) and further developed by Clarke & Delale (1986), and which has successfully been applied to subcritical and supercritical nozzle flows (Delale, Schnerr & Zierep 1993 *a*, *b*) and to shock tube flows (Delale *et al.* 1995). Such a closed-form asymptotic solution of the condensation rate equation is necessary in order to identify the distinct condensation zones with detailed analytical structure along streamlines. In addition the solution for the flow field in each condensation zone can be predicted very accurately independent of the theories of nucleation and droplet growth to be employed, and the predictions can be compared to measurements mapped over the same regions. We present herein the asymptotic solution for subcritical Prandtl–Meyer flows with homogeneous condensation by asymptotic analysis of the condensation rate equation along streamlines. From this analysis we identify the condensation zones along streamlines in a manner analogous to quasi-one-dimensional nozzle flows (cf. Delale *et al.* 1993 *a*). In particular we determine in closed form the nucleation wave front, which corresponds to states of maximum nucleation along streamlines in the expansion fan. We construct an algorithm for the subcritical expansion of moist air around a sharp corner utilizing the classical nucleation theory and the Hertz–Knudsen droplet growth law. The results obtained are then compared with the measurements of Smith (1971). Despite satisfactory qualitative agreement, substantial quantitative disagreement is observed between the position of the nucleation wave front computed by the subcritical algorithm and the locations of the measured onset conditions. This is because the characteristics, or Mach lines, emanating from the corner intersect in the heat addition zones, showing clearly the existence of an embedded oblique shock wave that pushes the nucleation wave front upstream towards the onset measurements. This indicates the need for the computation of flows with an embedded shock wave (supercritical flows) which will not be discussed in this article.

2. Equations of motion

We consider the Prandtl–Meyer expansion of a condensable vapour (denoted by subscript v) with an inert carrier gas (denoted by subscript i) around a sharp corner O

https://doi.org/10.1017/S0022112097008379 Published online by Cambridge University Press

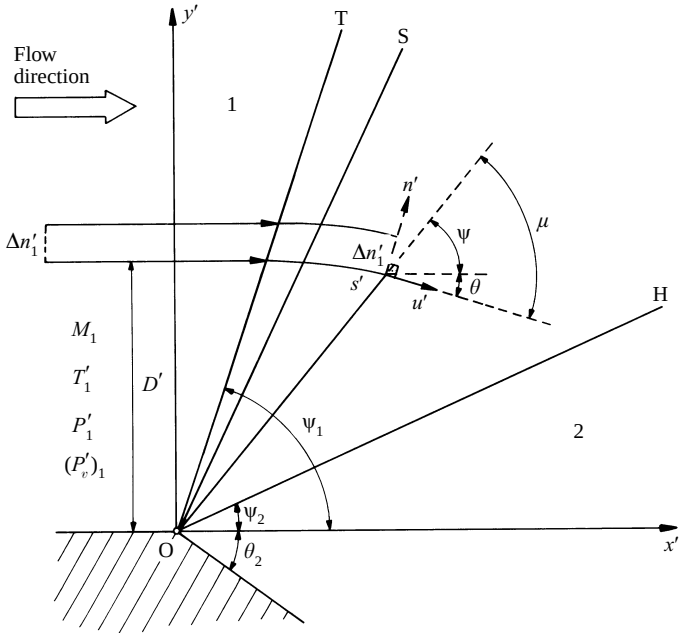


FIGURE 1. Configuration of streamlines and Mach lines in Prandtl–Meyer flows around a sharp corner located at the origin O of the (x', y')-plane (OT and OH are, respectively, the isentropic tail and head of the expansion fan, OS is the Mach line corresponding to saturated thermodynamic states and regions 1 and 2 denote, respectively, the uniform oncoming flow and the uniform flow downstream of the expansion fan).

between two uniform states separated by an expansion fan, as shown in figure 1. As soon as the flow crosses the saturation Mach line OS, where the vapour is saturated and before which no detectable condensation is observed, clusters of vapour molecules of the critical size for a tendency to growth (condensation nuclei) are produced by homogeneous nucleation. Rapid growth then sets in on the condensation nuclei to form droplets of various sizes. Consequently a non-equilibrium two-phase dispersed droplet flow with latent heat addition from condensation is created. Assuming that droplets move with the same velocity as the surrounding gas mixture (no velocity slip) and further that they are at the same temperature as that of the surrounding gas mixture (one-temperature model), the equations of motion for the non-equilibrium two-phase mixture can be written in the form corresponding to a single-phase flow of a homogeneous mixture with pressure p', density ρ', temperature T', flow speed u', flow direction θ (as shown in figure 1) and enthalpy h' (two-phase homogeneous dispersed droplet flow model). In what follows we discuss in detail the equations of motion of the two-phase mixture in this model.

2.1. *The flow and state equations in natural coordinates*

We consider the Euler equations for the steady two-dimensional supersonic flow of a mixture of a condensable vapour and a carrier gas in natural coordinates (s', n'), as shown in figure 1:

$$\frac{1}{\rho'}\frac{\partial \rho'}{\partial s'} + \frac{1}{u'}\frac{\partial u'}{\partial s'} - \frac{\partial \theta}{\partial n'} = 0, \tag{1}$$

https://doi.org/10.1017/S0022112097008379 Published online by Cambridge University Press

$$\rho' u' \frac{\partial u'}{\partial s'} = -\frac{\partial p'}{\partial s'}, \tag{2}$$

$$\rho' u'^2 \frac{\partial \theta}{\partial s'} = \frac{\partial p'}{\partial n'} \tag{3}$$

and

$$\rho' \frac{\partial h'}{\partial s'} = \frac{\partial p'}{\partial s'}. \tag{4}$$

The mixture enthalpy h' is related to the mixture temperature T' by

$$h' = c'_{pm} T' - gL'(T'), \tag{5}$$

where g, called the condensate mass fraction, is the ratio of the local mass flow rate of the condensed phase to that of the mixture along streamlines, $L'(T')$ is the latent heat of condensation corresponding to temperature T', and c'_{pm} is the specific heat of the mixture at constant pressure, given by

$$c'_{pm} = (1 - w_1) c'_{pi} + w_1 c'_{pv}, \tag{6}$$

with c'_{pi} and c'_{pv} denoting respectively the specific heats at constant pressure of the carrier gas and of the condensable vapour and with w_1 denoting the initial specific humidity (the mass fraction of the vapour component in the mixture) of the oncoming flow.

The thermal equation of state of the mixture, assumed to consist of ideal gases, follows by Dalton's law as

$$p' = p'_i + p'_v = \frac{\mathfrak{R}}{\mu_i} \rho'_i T' + \frac{\mathfrak{R}}{\mu_v} \rho'_v T', \tag{7}$$

where $\mathfrak{R} = 8.31441\ \mathrm{J\,mol^{-1}K^{-1}}$ is the universal gas constant, μ_i and μ_v are, respectively, the molecular masses of the carrier gas and of the condensable vapour, p'_i and p'_v are, correspondingly, the partial pressures of the carrier gas and of the condensable vapour, and ρ'_i and ρ'_v are, respectively, the partial densities of the carrier gas and of the condensable vapour and are related to the mixture density ρ' by the relations

$$\rho'_i = (1 - w_1) \rho' \tag{8}$$

and

$$\rho'_v = (w_1 - g) \rho'. \tag{9}$$

Using the above relations the thermal equation of state of the mixture takes the form

$$p' = \frac{\mathfrak{R}}{\mu_m} \left(1 - \frac{\mu_m}{\mu_v} g\right) \rho' T', \tag{10}$$

with the mixture molecular mass μ_m defined by

$$\frac{1}{\mu_m} \equiv \frac{1 - w_1}{\mu_i} + \frac{w_1}{\mu_v}. \tag{11}$$

We now conveniently normalize the flow variables p', ρ' and T' (from now on all variables with a prime are meant to denote physical values whereas those without a prime denote normalized values) as

$$p = \frac{p'}{p'_1}, \quad \rho = \frac{\rho'}{\rho'_1}, \quad T = \frac{T'}{T'_1}, \tag{12}$$

with subscript 1 denoting values of the oncoming flow, whereas the flow speed u', the

https://doi.org/10.1017/S0022112097008379 Published online by Cambridge University Press

mixture enthalpy h', the mixture specific heat at constant pressure c'_{pm} and the latent heat L' are normalized somewhat differently as

$$u = \frac{u'}{(\Re T'_1/\mu_m)^{1/2}},\ h = \frac{h'}{\Re T'_1/\mu_m},\ c_{pm} = \frac{c'_{pm}}{\Re/\mu_m} \quad \text{and} \quad L = \frac{L'}{\Re T'_1/\mu_v}. \tag{13}$$

The streamwise and normal coordinates s' and n' are also normalized with respect to a characteristic flow length ℓ' as

$$s = \frac{s'}{\ell'} \quad \text{and} \quad n = \frac{n'}{\ell'}. \tag{14}$$

Then the flow and state equations (1)–(4) and (10) take the normalized form

$$\frac{1}{\rho}\frac{\partial \rho}{\partial s} + \frac{1}{u}\frac{\partial u}{\partial s} - \frac{\partial \theta}{\partial n} = 0, \tag{15}$$

$$\rho u \frac{\partial u}{\partial s} = -\frac{\partial p}{\partial s}, \tag{16}$$

$$\rho u^2 \frac{\partial \theta}{\partial s} = \frac{\partial p}{\partial n}, \tag{17}$$

$$\rho \frac{\partial h}{\partial s} = \frac{\partial p}{\partial s}, \tag{18}$$

and

$$p = \left(1 - \frac{\mu_m}{\mu_v} g\right) \rho T \tag{19}$$

with the normalized mixture enthalpy h given by

$$h = c_{pm} T - g L(T). \tag{20}$$

These normalized flow and state equations (15)–(20) do not form a complete system unless they are supplemented by the condensation rate equation for the condensate mass fraction g.

2.2. *The condensation rate equation*

The condensation rate equation for g is constructed along a streamline from a nucleation rate equation and a droplet growth law (see e.g. Clarke & Delale 1988). For this purpose we consider a streamtube (with thickness unity perpendicular to the plane of flow) formed by two streamlines with arbitrarily small normal separation $\Delta n'_1$ in the uniform oncoming flow, as shown in figure 1. We let $m'_r(s'; \xi')$ denote the mass of a droplet of radius $r'(s'; \xi')$ at a point with streamwise coordinate s' created at some point with coordinate $\xi' \leqslant s'$ along the same streamline. We also let $\Delta n'(s')$ be the normal separation between the streamlines at s' and $J'(\xi')$ be the rate of production of clusters of critical radius $r^{*\prime}(\xi')$ per unit volume (nucleation rate) at some point ξ' along the streamlines. The integral condensation rate equation for g along streamlines can then be written as

$$g(s') \equiv \frac{\Delta m'_{con}}{\Delta m'} = \frac{1}{\Delta m'} \int_{s'_c}^{s'} m'_r(s'; \xi') \Delta n'(\xi') J'(\xi') \mathrm{d}\xi', \tag{21}$$

where $\Delta m'_{con}$ and $\Delta m'$ are respectively the dispersed liquid (condensed phase) and the mixture mass flow rates through the same streamtube, and where s'_c corresponds to

https://doi.org/10.1017/S0022112097008379 Published online by Cambridge University Press

the value of s' at which the streamline considered crosses the saturation Mach line OS.

Despite the fact that various theories of nucleation yield nucleation rates J' which are sometimes different by orders of magnitude in comparison with experiments, all can be cast into the common functional form

$$J' = \zeta' \Sigma(p, T, g) \exp\,[-K^{-1} B(p, T, g)]. \tag{22}$$

Here $B(p, T, g)$ is the normalized activation function and is $O(1)$ over regions where nucleation rates are significant, K is the nucleation parameter with magnitude much less than unity signifying a relatively large nucleation period to achieve significant nucleation rates, ζ' is a normalization constant for the nucleation rate and $\Sigma(p, T, g)$ is the normalized pre-exponential factor of order unity in magnitude. Equation (22) suggests that no specific choice of the functions Σ and B and of the parameters ζ' and K is required although they may vary considerably in different theories. Thus the analysis can be kept independent of the particular choice of the nucleation rate equation to be employed.

For the discussion of the droplet growth law, we first normalize the droplet radius r' by

$$r = \frac{r'}{r'_d}, \tag{23}$$

where the normalization constant is conveniently chosen as

$$r'_d = \left(\frac{3\rho'_1}{4\pi \rho'_{con} \ell' \zeta'} \left(\frac{\Re}{\mu_m} T'_1 \right)^{1/2} \right)^{1/3}, \tag{24}$$

with ρ'_{con} denoting the mean density of the condensate in the range of temperatures investigated. Assuming that the droplet growth rate is independent of the droplet radius under the conditions investigated, the droplet growth law can be cast into the normalized form

$$\frac{\partial r}{\partial s} = \lambda \Omega(p, T, g), \tag{25}$$

where Ω is the droplet growth function depending on the thermodynamic state of the mixture and $O(1)$ in magnitude, and λ is the droplet growth parameter. In particular, rapid droplet growth in the expansion fan, which corresponds to small droplet growth time compared to characteristic flow time, is characterized by $\lambda \gg 1$. The initial-value problem of (24) with initial value $r(\xi; \xi) = r^*(\xi)$ along streamlines can be solved by simple quadrature, resulting in the explicit normalized equation

$$r(s; \xi) = r^*(\xi) + \lambda \int_{\xi}^{s} \Omega(\eta) \mathrm{d}\eta, \tag{26}$$

where $r^* = r'^*/r'_d$ is the normalized critical radius. Noting that $m'_r(s'; \xi')$ and $\Delta m'$ in (21) are given by

$$m'_r(s'; \xi') = \tfrac{4}{3} \pi \rho'_{con} [r'(s'; \xi')]^3 \tag{27}$$

and

$$\Delta m' = \rho'_1 u'_1 \Delta n'_1 = \rho'\,(s') u'(s') \Delta n'(s'), \tag{28}$$

and using (22), (23) and (25) together with the normalization of the previous section,

https://doi.org/10.1017/S0022112097008379 Published online by Cambridge University Press

the integral condensation rate equation (21) takes the normalized form

$$g(s) = \int_{s_c}^{s} \left[r^*(\xi) + \lambda \int_{\xi}^{s} \Omega(\eta) \mathrm{d}\eta \right]^3 \frac{\Sigma(\xi)}{\rho(\xi) u(\xi)} \exp[-K^{-1} B(\xi)] \mathrm{d}\xi \tag{29}$$

along streamlines.

2.3. *Alternative forms of the equations of motion*

Despite the fact that (15)–(20) together with the condensation rate equation (29) form a complete integro-differential system for determining the flow field, alternative forms of these equations may be useful in finding some particular or approximate solutions valid under specific conditions. For this reason we present two more forms, which will be used in obtaining particular solutions. We first discuss the form which the equations take along a streamtube constructed from two adjacent streamlines separated at the normalized streamwise coordinate s by the normalized normal distance $\Delta n(s) \equiv \Delta n'(s')/\ell'$ with arbitrarily small initial normalized normal separation Δn_1. Utilizing the geometric relation

$$\frac{\partial \theta}{\partial n} = -\frac{1}{\Delta n} \frac{\partial \Delta n}{\partial s}, \tag{30}$$

equations (15)–(20) can be conveniently cast into the integrated form

$$\rho u A = u_1, \tag{31}$$

$$(p + \rho u^2) A = 1 + u_1^2 + \mathscr{R}(s), \tag{32}$$

$$c_{pm} T + \tfrac{1}{2} u^2 - \frac{\mu_m}{\mu_v} L(T) g = c_{pm} + \tfrac{1}{2} u_1^2, \tag{33}$$

$$p = \rho T \left(1 - \frac{\mu_m}{\mu_v} g \right) \tag{34}$$

along streamlines. In (31)–(34) the normalized area $A(s)$ and impulse function $\mathscr{R}(s)$ are defined by

$$A(s) = \frac{\Delta n(s)}{\Delta n_1} \tag{35}$$

and

$$\mathscr{R}(s) = \int_0^s p(\xi) \frac{\mathrm{d}A}{\mathrm{d}\xi} \mathrm{d}\xi, \tag{36}$$

with the normalized streamwise coordinate s being measured from the tail of the expansion fan OT (see figure 1); and the streamlines are given by their normalized curvatures $\kappa(s)$ as

$$\kappa(s) = \frac{\partial \theta}{\partial s} = \frac{1}{\rho u^2} \frac{\partial p}{\partial n}. \tag{37}$$

Equations (31)–(36) are identical with the normalized equations of quasi-one-dimensional nozzle flows with non-equilibrium condensation (Blythe & Shih 1976; Clarke & Delale 1986) provided that s is replaced by the nozzle axial coordinate and that $A(s)$ is assumed to act as the normalized cross-sectional area of the nozzle. This form of the equations of flow and state is particularly useful in cases where the streamlines (and thereby $A(s)$) are known *a priori* or can somehow be approximated.

The system of equations of flow and state can also be cast (Vincenti & Kruger 1965; Clarke & Delale 1988) into characteristic form with a single condensation rate

https://doi.org/10.1017/S0022112097008379 Published online by Cambridge University Press

equation, as

$$\rho u \mathrm{d}u + \mathrm{d}p = 0, \tag{38}$$

$$h + \tfrac{1}{2}u^2 = c_{pm}T - L(T)g + \tfrac{1}{2}u^2 = c_{pm} + \tfrac{1}{2}u_1^2, \tag{39}$$

$$u\mathrm{d}g - \varpi \mathrm{d}s = 0 \tag{40}$$

on streamlines, and

$$\left(\frac{u^2}{a_f^2} - 1\right)^{1/2} \mathrm{d}p \pm \rho u^2 \mathrm{d}\theta - \frac{h_g}{h_\rho} a_f \varpi \begin{pmatrix} \mathrm{d}\eta \\ \mathrm{d}\zeta \end{pmatrix} = 0 \tag{41}$$

on the characteristic lines

$$\frac{\mathrm{d}n}{\mathrm{d}s} = \mp \frac{1}{((u^2/a_f^2) - 1)^{1/2}}, \tag{42}$$

together with the thermal equation of state (19) valid everywhere in the flow field. We have here defined the normalized local frozen speed of sound a_f by

$$a_f^2 = -\frac{h_\rho}{h_p - (1/\rho)} = \frac{[c_{pm} - (\mu_m/\mu_v)L_1 g]p}{\rho[c_{pm} - 1 + (\mu_m/\mu_v)(1 - L_1)g]}, \tag{43}$$

where the various partial derivatives of the normalized specific mixture enthalpy h evaluate to

$$h_p = \frac{[c_{pm} - (\mu_m/\mu_v)L_1 g]}{\rho[1 - (\mu_m/\mu_v)g]}, \tag{44}$$

$$h_\rho = -\frac{p[c_{pm} - (\mu_m/\mu_v)L_1 g]}{\rho^2[1 - (\mu_m/\mu_v)g]}, \tag{45}$$

$$h_g = \frac{(\mu_m/\mu_v)p[c_{pm} - (\mu_m/\mu_v)L_1 g]}{\rho[1 - (\mu_m/\mu_v)g]^2} - \frac{\mu_m}{\mu_v}L(T), \tag{46}$$

with $L_1 \equiv \mathrm{d}L/\mathrm{d}T$, and where the coordinates η and ζ are given by the transformation

$$\begin{pmatrix} \mathrm{d}/\mathrm{d}\eta \\ \mathrm{d}/\mathrm{d}\zeta \end{pmatrix} = \frac{(u^2 - a_f^2)^{1/2}}{u}\frac{\partial}{\partial s} \mp \frac{a_f}{u}\frac{\partial}{\partial n}. \tag{47}$$

In addition it is understood that the rate equation (40) along streamlines is to be obtained by direct differentiation from (29) with ϖ defined by

$$\varpi = r^{*3}(s)\frac{\Sigma(s)}{\rho(s)}\exp[-K^{-1}B(s)] + 3\lambda\Omega(s)u(s)\int_{s_c}^{s}\left[r^*(\xi) + \lambda\int_{\xi}^{s}\Omega(\eta)\mathrm{d}\eta\right]^2 \frac{\Sigma(\xi)}{\rho(\xi)u(\xi)}\exp[-K^{-1}B(\xi)]\mathrm{d}\xi \tag{48}$$

on streamlines.

3. Particular analytical solutions of the equations of motion

We discuss here two analytical solutions to the equations of motion using the alternative forms given in § 2.3. The first is the classical isentropic solution and is discussed solely for notational convenience. The second is an approximate solution valid for nearly frozen flows. Both will be useful in the asymptotic solution to be discussed in the next section.

https://doi.org/10.1017/S0022112097008379 Published online by Cambridge University Press

3.1. *The classical isentropic solution*

It is well-known that for isentropic flow ($g \equiv 0$) equation (41) yields the Riemann invariants

$$\omega(M) \pm \theta = \text{constant} \tag{49}$$

on the characteristic lines

$$\frac{\mathrm{d}n}{\mathrm{d}s} = \tan\mu = \pm\frac{1}{(M^2-1)^{1/2}} \tag{50}$$

where M is the isentropic Mach number, μ is the angle between the characteristic lines and streamlines (see figure 1) and $\omega(M)$ is the Prandtl–Meyer function defined by

$$\omega(M) = \left(\frac{\gamma+1}{\gamma-1}\right)^{1/2} \tan^{-1}\left(\frac{(\gamma-1)}{(\gamma+1)}(M^2-1)\right)^{1/2} - \tan^{-1}\left(M^2-1\right)^{1/2}, \tag{51}$$

with $\gamma = c_{pm}/(c_{pm}-1)$ denoting the adiabatic exponent of the mixture.

For a given oncoming uniform flow with Mach number M_1 and flow direction $\theta_1 = 0$ expanding around a sharp corner with angle θ_2 at the origin of the (x, y)-plane (see figure 1), it follows that

$$\omega(M) - \theta = \omega(M_1) \tag{52}$$

everywhere. The angles of inclination ψ_1 and ψ_2, in the (x, y)-plane of figure 1, of the tail OT and head OH of the isentropic rarefaction wave are then evaluated from the relations $\psi_1 = \sin^{-1}(1/M_1)$ and $\psi_2 = \sin^{-1}(1/M_2) - \theta_2$ where M_2 is found from $\omega(M_2) = \omega(M_1) + \theta_2$. The solution along any Mach line with inclination angle ψ in the rarefaction wave is obtained by first solving for the Mach number M from $\omega(M) - \sin^{-1}(1/M) = \omega(M_1) - \psi$ and for the flow direction θ from $\theta = \sin^{-1}(1/M) - \psi$, and then using the expressions that relate the rest of the flow variables to the Mach number. The solution thus obtained is self-similar, depending only on the single coordinate ψ, which identifies the particular Mach line.

3.2. *Solution for nearly frozen flows*

We now return to the alternative formulation given by (31)–(37) for the flow through a streamtube formed by two adjacent streamlines with arbitrarily small initial separation. We introduce nearly frozen flows by assuming weak coupling between the flow equations together with the thermal equation of state and the condensation rate equation. In this case the latent heat addition by condensation hardly influences the frozen (isentropic) network of streamlines, so that the area $A(s)$ and the streamline curvature $\kappa(s)$ defined, respectively, by (35) and (37), can be approximated by the frozen relations

$$A(s) = \frac{M_1}{M}\left[\frac{1+(\gamma-1)M^2/2}{1+(\gamma-1)M_1^2/2}\right]^{(\gamma+1)/2(\gamma-1)} \tag{53}$$

and

$$\kappa(s) = \kappa_f(s), \tag{54}$$

where $\kappa_f(s)$ denotes the curvature of the frozen streamlines under consideration. Furthermore, it can be shown that for nearly frozen flows the differences between the impulse function $\mathscr{R}(s)$ and its frozen value $\mathscr{R}_f(s)$, and between the latent heat $L(T)$ and its frozen value $L(T_f)$, are *each of second order or higher* compared with the (first order) deviations of the flow variables from their frozen (isentropic) values

https://doi.org/10.1017/S0022112097008379 Published online by Cambridge University Press

(Clarke & Delale 1986; Delale *et al.* 1993*a*), so that the approximations

$$\mathscr{R}(s) \approx \mathscr{R}_f(s) = \frac{M_1}{M}\left(\frac{1+(\gamma-1)M_1^2/2}{1+(\gamma-1)M^2/2}\right)^{1/2}(1+\gamma M^2)-(1+\gamma M_1^2) \tag{55}$$

and

$$L(s) \approx L_f(s) \equiv L(T_f) \tag{56}$$

hold along streamlines for nearly frozen flows. Equations (31)–(37) together with the approximations given by (53)–(56) form the flow and state equations for nearly frozen flows. These equations are precisely those for quasi-one-dimensional nearly frozen nozzle flows (Clarke & Delale 1986), and yield the functional relations

$$u(g,s) = \frac{2\gamma\{[1+u_1^2+\mathscr{R}_f(s)]/(2u_1)+[\Delta(g,s)]^{1/2}\}}{[\gamma+1+(\gamma-1)g\mu_m/\mu_v]}, \tag{57}$$

$$\rho(g,s) = \frac{u_1}{u(g,s)A(s)}, \tag{58}$$

$$p(g,s) = \frac{1+u_1^2+\mathscr{R}_f(s)-u_1u(g,s)}{A(s)} \tag{59}$$

and

$$T(g,s) = 1+\frac{u_1^2-u^2(g,s)}{2c_{pm}}+\frac{\mu_m}{\mu_v}\frac{L_f(s)g}{c_{pm}}, \tag{60}$$

with $\Delta(g,s)$ defined by

$$\Delta(g,s) \equiv \left[\frac{1+u_1^2+\mathscr{R}_f(s)}{2u_1}\right]^2 - \left[\frac{\gamma+1+(\gamma-1)g\mu_m/\mu_v}{2\gamma}\right]\left(1-\frac{\mu_m}{\mu_v}g\right)\left(1+\frac{u_1^2}{2c_{pm}}+\frac{\mu_m}{\mu_v}\frac{L_f(s)g}{c_{pm}}\right) \tag{61}$$

on streamlines, where $A(s)$, $\mathscr{R}_f(s)$ and $L_f(s)$ are, respectively, given by (53), (55) and (56). It follows from (57) that $\Delta(g,s)=0$ corresponds to the critical flow condition at which the amount of heat added to the flow along streamlines reaches the nearly frozen critical amount. As a matter of fact the nearly frozen approximation becomes invalid before such a condition can be reached; therefore, $\Delta(g,s)$ remains positive for nearly frozen flows. The functional relations (57)–(61) together with the asymptotic solution of the condensation rate equation (29) provide a complete analytical solution along streamlines for nearly frozen flows.

4. Asymptotic solution for subcritical flows

The asymptotic solution for subcritical Prandtl–Meyer flows with homogeneous condensation follows by combining the local solution of the equations of flow and state with the asymptotic solution of the condensation rate equation along streamlines. The latter is obtained in the double limit as $K \to 0$ and then $\lambda \to \infty$ characterizing, respectively, large nucleation period to achieve significant nucleation rates followed by small droplet growth time compared with the characteristic flow time. In particular the behaviour of the activation function $B(s)$ in (29) plays a dominant role in identifying the distinct condensation zones along streamlines. A typical variation of the activation function B along streamlines is shown in figure 2. For $s \leqslant s_c$, where s_c denotes the streamwise coordinate where the saturation line OS of the vapour is traversed,

https://doi.org/10.1017/S0022112097008379 Published online by Cambridge University Press

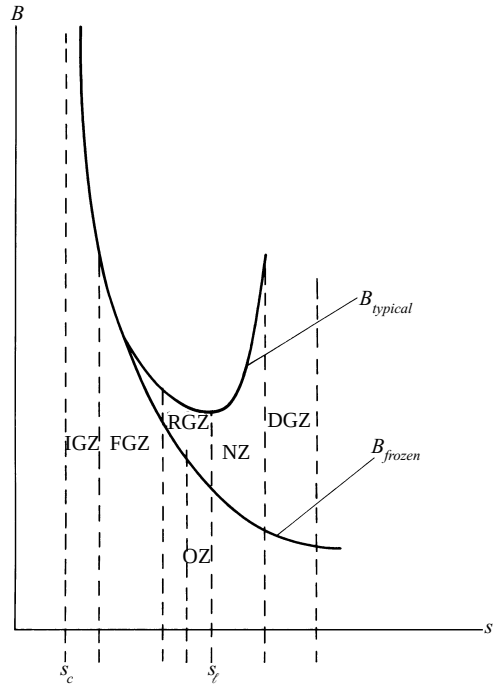


FIGURE 2. The variation of the normalized activation function B along a streamline in subcritical Prandtl–Meyer flows, exhibiting the physically distinct condensation zones (s_c is the streamwise location where saturation is reached and s_ℓ is the turning point of B).

the activation function B is infinite, corresponding to vanishing nucleation rates. It decreases (corresponding to increasing nucleation rates) until it reaches a turning point at $s = s_\ell$ where $\mathrm{d}B/\mathrm{d}s = 0$ and the nucleation rate is practically maximum. Downstream of the turning point, for $s > s_\ell$, the activation function B increases rapidly, causing the nucleation rate to fall rapidly due to significant heat addition from condensation. Further downstream nucleation practically terminates and droplet growth causes the two-phase mixture to relax towards saturated equilibrium states. Heat addition along any streamline is practically negligible in the interval $s_c \leqslant s \leqslant s_\ell$ (nearly frozen flows), whereas for $s > s_\ell$ a considerable amount of heat is released, resulting in highly compressed flow regions (heat addition zones).

4.1. *Nearly frozen zones*

These condensation zones can be distinguished along streamlines in the interval $s_c \leqslant s \leqslant s_\ell$ where the flow field is nearly frozen. Both nucleation and droplet growth are important in these zones; however, the influence of latent heat addition on the flow field in these zones seems negligible except for the onset zone (OZ), a very narrow zone just upstream of the turning point $s = s_\ell$ of B. From the behaviour of the activation function B in the nearly frozen interval $s_c \leqslant s \leqslant s_\ell$ (figure 2), one can identify four physically distinct zones in this interval. These are the initial growth zone (IGZ), the further growth zone (FGZ), the rapid growth zone (RGZ) and the onset zone (OZ). Of these physically distinct zones, the first two are not asymptotically distinct, and neither are the last two. Thus the asymptotic solution of the rate equation (29) for these zones can be carried out in a combined fashion.

In the initial and further growth zones, $\mathrm{d}B/\mathrm{d}s = O(1)$. They are distinguished

https://doi.org/10.1017/S0022112097008379 Published online by Cambridge University Press

physically. In IGZ no influence of the heat released by condensation on the flow field can be found, so that all of the flow variables and thermodynamic functions assume their frozen (isentropic) values, i.e. $p = p_f$, $\rho = \rho_f$, $T = T_f$, $B = B_f$, $\Omega = \Omega_f$, etc. This is the only zone where the flow and state equations are decoupled from the condensation rate equation. Within FGZ, deviations in B and its derivative $\mathrm{d}B/\mathrm{d}s$ from their frozen values B_f and $\mathrm{d}B_f/\mathrm{d}s$ start to occur because of latent heat addition from growing droplets, despite the fact that these deviations are not significant enough to influence the frozen field appreciably; however, the magnitudes of these deviations at the beginning and end of this zone differ significantly. Actually the initial growth zone (IGZ), where these deviations are exponentially small and can be totally neglected, can be thought of as being embedded in the further growth zone (FGZ). The combined asymptotic expressions for g and $\mathrm{d}g/\mathrm{d}s$ along streamlines in these zones then follow from (29) using Laplace's method (Erdelyi 1956; Sirovich 1971) for an end-point minimum in the double limit as $K \to 0$ and $\lambda \to \infty$ (for details see Delale *et al.* 1993 *a*):

$$g(s) = \frac{\Sigma(s)}{\rho(s)u(s)} K^4 \left(\frac{\mathrm{d}B}{\mathrm{d}s}\right)^{-4} \exp[-K^{-1}B(s)] \left\{ 6\lambda^3\Omega^3(s) - 6\lambda^2\Omega^2(s)\left[\frac{r^*(s)\mathrm{d}B/\mathrm{d}s}{K}\right] + 3\lambda\Omega(s)\left[\frac{r^*(s)\mathrm{d}B/\mathrm{d}s}{K}\right]^2 - \left[\frac{r^*(s)\mathrm{d}B/\mathrm{d}s}{K}\right]^3 \right\} \quad (62)$$

and

$$\frac{\mathrm{d}g}{\mathrm{d}s} = -\frac{\Sigma(s)}{\rho(s)u(s)} K^3 \left(\frac{\mathrm{d}B}{\mathrm{d}s}\right)^{-3} \exp[-K^{-1}B(s)] \left\{ 6\lambda^3\Omega^3(s) - 6\lambda^2\Omega^2(s)\left[\frac{r^*(s)\mathrm{d}B/\mathrm{d}s}{K}\right] + 3\lambda\Omega(s)\left[\frac{r^*(s)\mathrm{d}B/\mathrm{d}s}{K}\right]^2 - \left[\frac{r^*(s)\mathrm{d}B/\mathrm{d}s}{K}\right]^3 \right\}, \quad (63)$$

with $\mathrm{d}B/\mathrm{d}s$ given by

$$\frac{\mathrm{d}B}{\mathrm{d}s} = \frac{\partial B}{\partial p}\frac{\mathrm{d}p}{\mathrm{d}s} + \frac{\partial B}{\partial T}\frac{\mathrm{d}T}{\mathrm{d}s} + \frac{\partial B}{\partial g}\frac{\mathrm{d}g}{\mathrm{d}s}. \quad (64)$$

The asymptotic laws of growth given by (62) and (63) for the condensate mass fraction g and its derivative $\mathrm{d}g/\mathrm{d}s$ are violated as $\mathrm{d}B/\mathrm{d}s$ diminishes to $O(K^{1/2})$ as $K \to 0$, and then we are by definition in the rapid growth zone RGZ (see figure 2). The turning point s_ℓ of the activation function B, where $\mathrm{d}B/\mathrm{d}s = 0$ corresponding to a maximum nucleation rate, marks the end of this zone. The beginning of the collapse of the supersaturated vapour state (the onset or Wilson point s_k), which can either be detected empirically by light scattering or deduced by assigning numerically a value g_k for the condensate mass fraction at this point, occurs within this zone and marks the beginning of the onset of condensation. The region lying between the onset point s_k and the turning point s_ℓ of the activation function along streamlines is called the onset zone (OZ). Actually, the onset zone can be thought of as being embedded in RGZ. Although the onset zone can be distinguished physically from the very beginning of RGZ, these zones are not asymptotically distinct. In finding the asymptotic solution of the condensation rate equation (29) in these zones by Laplace's method for an end-point minimum, it is important to mention that the activation function $B(\xi)$ can no longer be truncated at the end-point $\xi = s$ after the second term

https://doi.org/10.1017/S0022112097008379 Published online by Cambridge University Press

$\mathrm{d}B/\mathrm{d}s(\xi - s)$, as was done in FGZ, since the third term $(1/2)\mathrm{d}^2B/\mathrm{d}s^2(\xi - s)^2$ (and in some anomalous cases even higher-order terms) may become of the same order of magnitude as the second term. The asymptotic expressions for g and its derivatives $\mathrm{d}g/\mathrm{d}s$ and $\mathrm{d}^2g/\mathrm{d}s^2$ in these zones, taking into account only the third-term correction, then follow by Laplace's method for an end-point minimum in the double limit as $K \to 0$ and $\lambda \to \infty$ (for details see Delale *et al.* 1993 *a*):

$$g(s) = \frac{\Sigma(s)}{\rho(s)u(s)}[2\beta(s)]^{-2}\exp\left[\frac{\gamma^2(s)}{8\beta(s)}\right]\exp[-K^{-1}B(s)]$$
$$\times\left\{6\lambda^3\Omega^3(s)D_{-4}\left[\frac{\gamma(s)}{(2\beta(s))^{1/2}}\right] + 6\lambda^2\Omega^2(s)[r^*(s)(2\beta(s))^{1/2}]D_{-3}\left[\frac{\gamma(s)}{(2\beta(s))^{1/2}}\right]\right.$$
$$\left.+3\lambda\Omega(s)[r^*(s)(2\beta(s))^{1/2}]^2D_{-2}\left[\frac{\gamma(s)}{(2\beta(s))^{1/2}}\right] + [r^*(s)(2\beta(s))^{1/2}]^3D_{-1}\left[\frac{\gamma(s)}{(2\beta(s))^{1/2}}\right]\right\}, \tag{65}$$

$$\frac{\mathrm{d}g}{\mathrm{d}s} = \frac{\Sigma(s)}{\rho(s)u(s)}[2\beta(s)]^{-3/2}\exp\left[\frac{\gamma^2(s)}{8\beta(s)}\right]\exp[-K^{-1}B(s)]$$
$$\times\left\{6\lambda^3\Omega^3(s)D_{-3}\left[\frac{\gamma(s)}{(2\beta(s))^{1/2}}\right] + 6\lambda^2\Omega^2(s)[r^*(s)(2\beta(s))^{1/2}]D_{-2}\left[\frac{\gamma(s)}{(2\beta(s))^{1/2}}\right]\right.$$
$$\left.+3\lambda\Omega(s)[r^*(s)(2\beta(s))^{1/2}]^2D_{-1}\left[\frac{\gamma(s)}{(2\beta(s))^{1/2}}\right] + [r^*(s)(2\beta(s))^{1/2}]^3\exp\left[-\frac{\gamma^2(s)}{8\beta(s)}\right]\right\}, \tag{66}$$

and

$$\frac{\mathrm{d}^2g}{\mathrm{d}s^2} = \frac{1}{\Omega(s)}\frac{\mathrm{d}\Omega}{\mathrm{d}s}\frac{\mathrm{d}g}{\mathrm{d}s}$$
$$+\frac{\Sigma(s)}{\rho(s)u(s)}[2\beta(s)]^{-1}\exp\left[\frac{\gamma^2(s)}{8\beta(s)}\right]\exp[-K^{-1}B(s)]$$
$$\times\left\{6\lambda^3\Omega^3(s)D_{-2}\left[\frac{\gamma(s)}{(2\beta(s))^{1/2}}\right] + 6\lambda^2\Omega^2(s)[r^*(s)(2\beta(s))^{1/2}]D_{-1}\left[\frac{\gamma(s)}{(2\beta(s))^{1/2}}\right]\right.$$
$$+3\lambda\Omega(s)[r^*(s)(2\beta(s))^{1/2}]^2\exp\left[-\frac{\gamma^2(s)}{8\beta(s)}\right] + [r^*(s)(2\beta(s))^{1/2}]^3\exp\left[-\frac{\gamma^2(s)}{8\beta(s)}\right]$$
$$\left.\times\left[\frac{3}{r^*(s)}\frac{\mathrm{d}r^*}{\mathrm{d}s} + \frac{1}{\Sigma(s)}\frac{\mathrm{d}\Sigma}{\mathrm{d}s} - \frac{1}{\rho(s)}\frac{\mathrm{d}\rho}{\mathrm{d}s} - \frac{1}{u(s)}\frac{\mathrm{d}u}{\mathrm{d}s} - \frac{1}{\Omega(s)}\frac{\mathrm{d}\Omega}{\mathrm{d}s} + \gamma(s)\right]/(2\beta(s))^{1/2}\right\}, \tag{67}$$

where $D_{-v}(z), v = 1, 2, 3, 4$ is Whittaker's parabolic cylinder function of z (Abramowitz & Stegun 1965; Gradshteyn & Ryzhik 1980),

$$\gamma(s) \equiv -K^{-1}\frac{\mathrm{d}B}{\mathrm{d}s} \geqslant 0 \tag{68}$$

and

$$\beta(s) \equiv \tfrac{1}{2}K^{-1}\frac{\mathrm{d}^2B}{\mathrm{d}s^2} > 0 \tag{69}$$

https://doi.org/10.1017/S0022112097008379 Published online by Cambridge University Press

with $\mathrm{d}B/\mathrm{d}s$ evaluated from (64) and $\mathrm{d}^2B/\mathrm{d}s^2$ given by

$$\frac{\mathrm{d}^2B}{\mathrm{d}s^2} = \frac{\partial B}{\partial p}\frac{\mathrm{d}^2p}{\mathrm{d}s^2} + \frac{\partial B}{\partial T}\frac{\mathrm{d}^2T}{\mathrm{d}s^2} + \frac{\partial B}{\partial g}\frac{\mathrm{d}^2g}{\mathrm{d}s^2} + \frac{\partial^2 B}{\partial p^2}\left(\frac{\mathrm{d}p}{\mathrm{d}s}\right)^2 + \frac{\partial^2 B}{\partial T^2}\left(\frac{\mathrm{d}T}{\mathrm{d}s}\right)^2 + \frac{\partial^2 B}{\partial g^2}\left(\frac{\mathrm{d}g}{\mathrm{d}s}\right)^2 + 2\left(\frac{\partial^2 B}{\partial p\partial T}\frac{\mathrm{d}p}{\mathrm{d}s}\frac{\mathrm{d}T}{\mathrm{d}s} + \frac{\partial^2 B}{\partial p\partial g}\frac{\mathrm{d}p}{\mathrm{d}s}\frac{\mathrm{d}g}{\mathrm{d}s} + \frac{\partial^2 B}{\partial T\partial g}\frac{\mathrm{d}T}{\mathrm{d}s}\frac{\mathrm{d}g}{\mathrm{d}s}\right). \quad (70)$$

The asymptotic expression for g and its derivatives along streamlines at s_ℓ then follow in the limit as $\gamma \to \gamma_\ell \equiv 0$, $\beta \to \beta_\ell$, $\Sigma \to \Sigma_\ell$, etc. where by subscript ℓ we mean evaluation at the turning point $s = s_\ell$.

The flow field in each zone is obtained by combining the asymptotic expressions for g and its derivatives exhibited above with the nearly frozen solution of § 3.2. As mentioned earlier, in IGZ the nearly frozen solution for the flow field reduces to the classical isentropic solution given in § 3.1. The condensate mass fraction g and its derivative $\mathrm{d}g/\mathrm{d}s$ in IGZ, both exponentially small in order of magnitude, are in turn evaluated from the asymptotic expressions (62) and (63) by replacing all of the thermodynamic functions by their frozen values. In FGZ, RGZ and OZ the solution at any point along streamlines can be obtained iteratively by utilizing the nearly frozen functional relations (57)–(61) and the asymptotic expressions given above. This iterative scheme is fairly simple. On any streamline we first use the local frozen solution to calculate g and its derivatives from (62)–(64) in FGZ and from (65)–(70) in RGZ and OZ. Substitution of these values for g into the functional relations then yields the first iterative approximation for the flow field. Using these first iterates for the flow field, we correct for the thermodynamic functions, in particular for $\mathrm{d}B/\mathrm{d}s$ and $\mathrm{d}^2B/\mathrm{d}s^2$. Substitution of these corrected values into (62)–(64) in FGZ and into (65)–(70) in RGZ and OZ yields new iterates for g and its derivatives. Inserting these values into the functional relations (57)–(61) yields the second iterative approximation for the flow field (usually a single iteration suffices). The theoretical onset point s_ℓ, that marks the end of the onset zone with a maximum nucleation rate, can now be identified as the point where

$$\left(\frac{\mathrm{d}B}{\mathrm{d}s}\right)_{s=s_\ell} = 0. \quad (71)$$

By repeating the procedure for different streamlines, we obtain the locus of theoretical onset points which we will refer to as the nucleation wave front (curve EF in figure 3).

4.2. *Heat addition zones*

Along any streamline downstream of the onset zone ($s > s_\ell$), the effect of heat addition to the flow can no longer be taken into account by the nearly frozen approximation of § 4.1. In this case a new solution to the flow field should be sought. Considering the integral condensation rate equation (29) downstream of the onset zone, two asymptotically and physically distinct zones can be distinguished. These are the nucleation zone with growth (NZ), where both nucleation and droplet growth are important, and the droplet growth zone (DGZ) which is dominated by droplet growth (see figure 2). The nucleation zone with growth (NZ) meets the onset zone (OZ) on the nucleation wave front EF (see figure 3) and extends downstream on a streamline until nucleation becomes negligible for any practical purpose. The effect of heat addition on the flow field can now be felt much more strongly, showing an increase in the pressure, density and temperature of the mixture over the thickness of the zone. Using Laplace's method for an interior minimum at $s = s_\ell$ in the limit as

https://doi.org/10.1017/S0022112097008379 Published online by Cambridge University Press

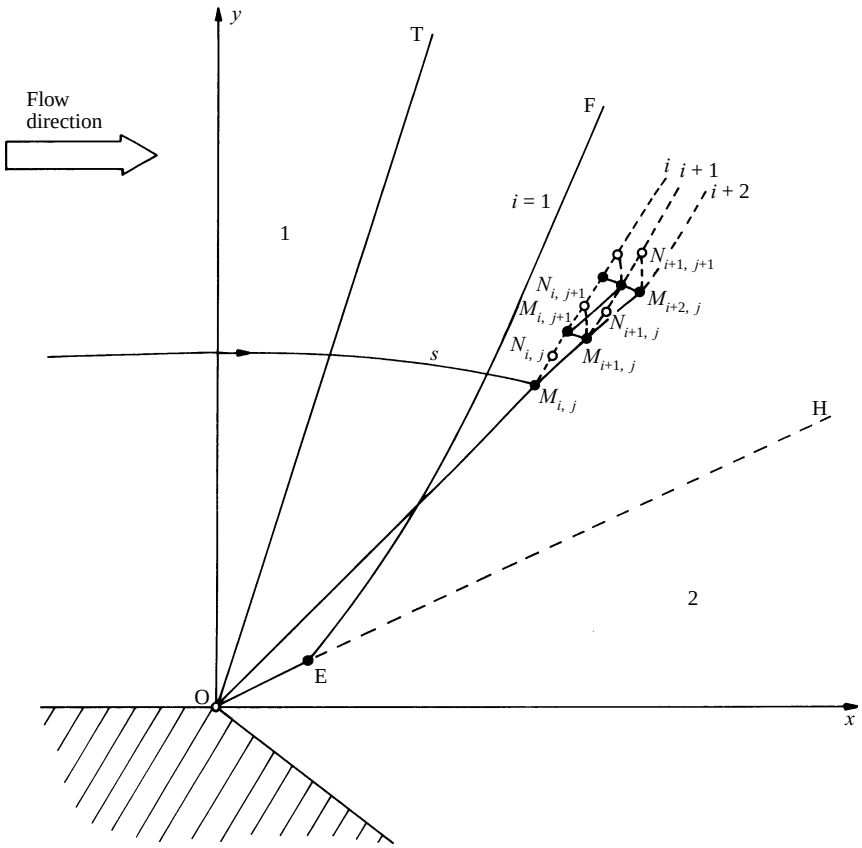


FIGURE 3. Construction of the network of characteristics for the asymptotic solution in the heat addition zones (EF is the nucleation wave front, OT is the tail of the expansion fan and OH is the isentropic (virtual) head of the expansion fan).

$K \to 0$ and then $\lambda \to \infty$, the condensation rate equation (29) in this zone yields the asymptotic expressions (details are given in Delale *et al.* 1993 *a*)

$$g(s) = b_\ell[(r_\ell^* + a_\ell\phi)^3 F_0(\phi) - 3a_\ell(r_\ell^* + a_\ell\phi)^2 F_1(\phi) + 3a_\ell^2(r_\ell^* + a_\ell\phi)F_2(\phi) - a_\ell^3 F_3(\phi)], \quad (72)$$

$$\varpi(s) \equiv u(s)\frac{\mathrm{d}g}{\mathrm{d}s} = r^{*3}(s)\frac{\Sigma(s)}{\rho(s)}\exp[-K^{-1}B(s)]$$
$$+3\lambda\Omega(s)u(s)b_\ell\left\{(r_\ell^* + a_\ell\phi)^2 F_0(\phi) - 2a_\ell(r_\ell^* + a_\ell\phi)F_1(\phi) + a_\ell^2 F_2(\phi)\right\}, \quad (73)$$

where the scaled coordinate ϕ and the constants a_ℓ and b_ℓ are given by

$$\phi \equiv \beta_\ell^{1/2}(s - s_\ell) \geqslant 0, \quad (74)$$

$$a_\ell \equiv \lambda\Omega_\ell\beta_\ell^{-1/2}, \quad (75)$$

$$b_\ell \equiv \frac{\Sigma_\ell}{\rho_\ell u_\ell}\beta_\ell^{-1/2}\exp[-K^{-1}B_\ell], \quad (76)$$

https://doi.org/10.1017/S0022112097008379 Published online by Cambridge University Press

with subscript ℓ denoting values at $s = s_\ell$ and where the functions $F_k(\phi)$ $(k = 0, 1, 2, 3)$ are defined by

$$F_0(\phi) \equiv \tfrac{1}{2}\pi^{1/2}(1 + \mathrm{erf}\phi), \tag{77}$$

$$F_1(\phi) \equiv -\tfrac{1}{2}\mathrm{e}^{-\phi^2}, \tag{78}$$

$$F_2(\phi) \equiv \tfrac{1}{4}\pi^{1/2}(1 + \mathrm{erf}\phi) - \tfrac{1}{2}\phi\mathrm{e}^{-\phi^2}, \tag{79}$$

and

$$F_3(\phi) \equiv -\tfrac{1}{2}(\phi^2 + 1)\mathrm{e}^{-\phi^2} \tag{80}$$

with $\mathrm{erf}\phi$ denoting the conventional error function. In particular, in the far field of this zone (as $\phi \to \infty$) we obtain the asymptotic expressions

$$g \sim \pi^{1/2} b_\ell a_\ell^3 \left\{ \phi^3 + 3\left(\frac{r_\ell^*}{a_\ell}\right)\phi^2 + 3\left[\frac{1}{2} + \left(\frac{r_\ell^*}{a_\ell}\right)^2\right]\phi + \left(\frac{r_\ell^*}{a_\ell}\right)^3 + \frac{3}{2}\left(\frac{r_\ell^*}{a_\ell}\right) \right\} \tag{81}$$

and

$$\varpi \sim 3\pi^{1/2}\lambda\Omega(s)u(s)b_\ell a_\ell^2\left[\phi^2 + 2\left(\frac{r_\ell^*}{a_\ell}\right)\phi + \left(\frac{r_\ell^*}{a_\ell}\right)^2 + \frac{1}{2}\right]. \tag{82}$$

These expressions, which correspond to linear growth of the droplet radius with the streamwise coordinate, cannot persist downstream of this zone where the two-phase mixture relaxes towards saturated equilibrium states. For this reason, downstream of NZ, we conveniently define the scaled variables $\bar{R}$ and χ along streamlines by

$$\bar{R} = \Lambda K^{-1/3} \int_{s_\ell}^{s} \frac{\Omega(\eta)}{\Omega_\ell} \mathrm{d}\eta, \tag{83}$$

$$\chi = \Lambda K^{-1/3}(s - s_\ell), \tag{84}$$

with

$$\Lambda = (\pi^{1/2} b_\ell K)^{1/3}\lambda\Omega_\ell. \tag{85}$$

Using Laplace's variable for an interior minimum at $s = s_\ell$ in the double limit as $K \to 0$ and $\lambda \to \infty$, the condensation rate equation yields, in terms of the new streamwise coordinate χ,

$$g = \bar{R}^3 + \epsilon_2\bar{R}^2 + \epsilon_1\bar{R} + \epsilon_0 \tag{86}$$

and

$$\varpi = (\pi^{1/2} b_\ell)^{1/3}\lambda\Omega(s)u(s)(3\bar{R}^2 + 2\epsilon_2\bar{R} + \epsilon_1), \tag{87}$$

where

$$\epsilon_0 = \pi^{1/2} b_\ell [r_\ell^{*3} + \tfrac{3}{2}a_\ell^2 r_\ell^*], \tag{88}$$

$$\epsilon_1 = 3(\pi^{1/2} b_\ell)^{2/3}[r_\ell^{*2} + \tfrac{1}{2}a_\ell^2], \tag{89}$$

$$\epsilon_2 = 3(\pi^{1/2} b_\ell)^{1/3} r_\ell^*, \tag{90}$$

and where $\bar{R}$ satisfies the relaxation rate equation

$$\frac{\mathrm{d}\bar{R}}{\mathrm{d}\chi} = \bar{\Omega} = \frac{\Omega}{\Omega_\ell}, \tag{91}$$

with the initial condition $\bar{R} = 0$ at $\chi = 0$.

Now that we have obtained the asymptotic expressions for g and $\mathrm{d}g/\mathrm{d}s$ in the heat addition zones (NZ and DGZ), we can construct a semi-analytical solution

https://doi.org/10.1017/S0022112097008379 Published online by Cambridge University Press

by returning to the characteristic form given by (38)–(42). Let $M_{i,j}$ ($j = 1, 2, ...$) be points in the heat addition zones NZ or DGZ of the expansion wave on a given curve, labelled curve i in figure 3, where the flow field is assumed known (the initial curve $i = 1$ is taken as the nucleation wave front EF constructed from the nearly frozen solution). The aim is to locate by interpolation the points $M_{i+1,j}$, $j = 1, 2, \ldots$, which are points of intersection of the characteristic lines $M_{i,j}\,M_{i+1,j}$, $M_{i,j+1}\,M_{i+1,j}$ and $N_{i,j+1}\,M_{i+1,j}$, and to find the flow field at these points. Writing (38)–(40) along the streamline $M_{i,j+1}\,M_{i+1,j}$, equation (41) with the (+) sign along the characteristic line $M_{i,j}\,M_{i+1,j}$ and with the (−) sign along the characteristic line $N_{i,j+1}\,M_{i+1,j}$ together with the equations for characteristics given by (42) in finite difference form, and utilizing the local asymptotic expressions (72), (73) in NZ and (86), (87) in DGZ, we iteratively locate the points $N_{i,j+1}$ and $M_{i+1,j}$ ($j = 1, 2, ...$) and solve for the flow field at the points $M_{i+1,j}$ ($j = 1, 2, ...$). Starting with the initial curve $i = 1$ (the nucleation wave front) and repeating the same procedure for increasing i until complete relaxation of the rate equation (91) along streamlines is reached, we obtain the subcritical solution for the flow field in the heat addition zones NZ and DGZ.

The solution thus obtained yields a continuous solution for the flow field (subcritical flows) provided that the heat added to the flow does not exceed a critical value. Cases where this critical value is exceeded (supercritical flows) show embedded shock waves and need separate consideration.

5. Asymptotic predictions and comparison with experiments

Predictions of the subcritical asymptotic solution for Prandtl–Meyer flows with homogeneous condensation presented in the preceding sections can now be made by assuming a nucleation rate equation and a droplet growth law. For the condensation of water vapour with a carrier gas in the range of temperatures to be investigated, the classical nucleation rate equation and the Hertz–Knudsen droplet growth law, together with some poorly known thermodynamic functions such as surface tension and accommodation coefficient fitted to the recent experiments of Peters & Paikert (1989), have been shown to compare well with experimental data in nozzles (e.g. see Schnerr & Dohrmann 1990; Delale *et al.* 1993*a*). Thus we employ the same condensation model. As in the procedure given in Delale *et al.* (1993*a*), we cast the classical nucleation rate equation into the normalized form of (22) with

$$\zeta' = \left(\frac{1}{500\pi}\right)^{1/2}\left(\frac{T_1'}{100}\right)^4 (m')^{-3/2}\frac{w_1^2\rho_1'^{\,2}}{\rho_{con}'}, \tag{92}$$

$$\Sigma(p, T, g) = \left(\frac{f(T)}{T^3}\right)^{1/2}\left(\frac{1 - g/w_1}{1 - \mu_m/\mu_v g}\right)^2 p^2, \tag{93}$$

$$B(p, T, g) = [f(T)]^3[\ln S(p, T, g)]^{-2} \tag{94}$$

and

$$K = \frac{3\times 10^{15}}{16\pi}k^3\left(\frac{\rho_{con}'}{m'}\right)^2\left(\frac{100}{T_1'}\right)^9, \tag{95}$$

https://doi.org/10.1017/S0022112097008379 Published online by Cambridge University Press

where the normalized surface tension $f(T)$ and the supersaturation $S(p,T,g)$ are given by

$$f(T)=\begin{cases}(100/T_1')^4[76.1+0.155(273.15-T_1'T)/T] & \text{for} \quad T\geqslant 249.4/T_1' \\ (11.31-0.03709T_1'T)T^3 & \text{for} \quad T<249.4/T_1'\end{cases} \tag{96}$$

and

$$S(p,T,g)=\frac{p_1'\mu_m(w_1-g)}{T_1'^{2.4576}(\mu_v-\mu_m g)}\frac{p}{T^{2.4576}\exp[v_0+v_1T+v_2T^2+v_3/T]} \tag{97}$$

with $v_0=21.125$, $v_1=-2.7246\times10^{-2}T_1'$, $v_2=1.6853\times10^{-5}T_1'^2$ and $v_3=-6.095\times10^3/T_1'$. Moreover, in (92)–(97), m' is the mass of a single vapour molecule and $k=1.38\times10^{-23}$ J K^{-1} is Boltzmann's constant. Similarly (details are given in Delale *et al.* 1993 *a*) the Hertz–Knudsen droplet growth law can be cast into the normalized form of (25) with

$$\lambda=2\times10^{-4}\frac{\ell'}{r_d'}\frac{T_1'^{1.4576}(\mu_v\mu_m)^{1/2}}{(2\pi)^{1/2}\rho_{con}'\mathfrak{R}}, \tag{98}$$

$$\Omega(p,T,g)=5\times10^3\alpha(T)\frac{T^{1.9576}\exp[v_0+v_1T+v_2T^2+v_3/T]}{(2[c_{pm}(1-T)+u^2/2+(\mu_m/\mu_v)Lg])^{1/2}} \times[S(p,T,g)-1], \tag{99}$$

where the accommodation coefficient $\alpha(T)$ is given by

$$\alpha(T)=\begin{cases}0.5 & \text{for} \quad T>270/T_1' \\ 1-0.0125(T_1'T-230) & \text{for} \quad 230/T_1'\leqslant T\leqslant 270/T_1' \\ 1 & \text{for} \quad T<230/T_1'.\end{cases} \tag{100}$$

The normalized critical radius $r^*(p,T,g)$ can then be obtained from the normalized Gibbs–Thomson equation as

$$r^*(p,T,g)=\frac{2m'}{10^5r_d'\rho_{con}'k}\left(\frac{T_1'}{100}\right)^3\frac{f(T)}{\ln S(p,T,g)}. \tag{101}$$

With the above information, an algorithm for Prandtl–Meyer flows with subcritical heat addition from condensation can be developed for the expansion of moist air. The nucleation wave front (curve EF in figure 3) is precisely located using the asymptotic method described in the previous section, and the nearly frozen zones are identified along streamlines. The effect of heat addition on the flow field is computed semi-analytically in the heat addition zones. Using this algorithm, the subcritical asymptotic solution is compared with available experimental data for the expansion of moist air around a sharp corner. Unfortunately literature on experimental data in corner expansion flows with condensation is scarce. This may be due to the difficulty of realizing a Prandtl–Meyer flow in practice. Among experiments on corner expansion flows of moist air, we can cite those by Smith (1971) and more recently by Frank (1985). Since measured points of onset of condensation (which presumably lie in the onset zone (OZ) and form the so-called condensation wave front) are plotted in the physical plane and details of the experimental conditions are reported therein, we choose to compare the asymptotic predictions with the experiments of Smith (1971). In those experiments corner expansions with condensation were carried out in a Ludwieg tube intermittent supersonic wind tunnel producing a steady flow through a

https://doi.org/10.1017/S0022112097008379 Published online by Cambridge University Press

two-dimensional nozzle. A sharp corner with an angle of deviation of 40° was located on the lower nozzle block at the geometric nozzle throat. Stagnation properties at the nozzle entrance were computed from measured tunnel supply temperature, pressure and relative humidity using standard gas dynamic equations for Ludwieg tube operation. Interferograms of the expansion were made by a Mach–Zehnder interferometer and were analysed to obtain information on the onset of condensation and on the shape of the condensation front.

Before we compare the asymptotic predictions with measurements, it would be useful to discuss some of the difficulties in realizing the corner expansion flows of moist air in the experimental set-up of Smith (1971) outlined above. One difficulty is with the location of the sharp corner being taken at the throat of the nozzle, resulting in a supersaturated state ($S > 1$) of the condensable vapour in the oncoming flow conditions. This means that the oncoming flow for the Prandtl–Meyer expansion is already nucleating. Other difficulties arise in conjunction with the effect of the boundary layer near the corner, which produces deviations from isentropic flow, and also with the non-uniformity of the oncoming flow at the corner. It is well-known that for an expansion in a convergent–divergent nozzle, the gradients at the throat are finite (non-vanishing), resulting in a non-uniform flow at the throat where the corner is located. However, the oncoming flow in the Prandtl–Meyer expansion around a corner is assumed to be uniform. Thus we have to allow for discontinuities in the flow gradients at the throat (along the line $x' = 0$) if we are to proceed with the asymptotic solution of subcritical corner expansion flows as realized in a convergent–divergent nozzle experiment. The features discussed above show that a smooth variation of the activation function B over the whole length of the nozzle is not possible. A typical variation of B along streamlines for the experimental set-up of Smith (1971) is shown in figure 4, in contrast to the typical smooth variation of figure 2. The oncoming flow being non-uniform and already nucleating ($S > 1$) at the tail of the expansion fan gives rise to a singularity of the activation function there. This singularity not only induces a change in the slope of the activation function along a streamline, but it also leads to a change in the sign of the curvature of the activation function. Consequently, the activation function B has to pass through an inflection point located downstream of this singularity if it is to reach the turning point $s = s_\ell$ along the streamline. This, in turn, seems to result in a downstream shift of the onset zone (OZ) computed by the subcritical asymptotic solution as compared to that realized in the experiments of Smith (1971). In principle the contribution from the singularity in B could be calculated, using standard asymptotic arguments, if the derivatives of B on either side of the singular point were known. That information is, unfortunately, not available for Smith's (1971) experiments, where we have information about the oncoming flow at the throat section only. Another important difficulty in realizing ideal Prandtl–Meyer flows in the experimental set-up of Smith arises from the interference of waves reflected from the upper wall of the nozzle, as already mentioned by Smith (1971) himself.

With these difficulties in mind, we can now compare the predictions of the asymptotic theory against the onset measurements of Smith (1971), which were deduced by measuring changes in fringe curvature. Figure 5 shows the measured condensation wave fronts (measured onset conditions) and the nucleation wave fronts predicted by (71) in the physical (x', y')-plane for moist air expansions under two different nozzle supply conditions in the experiments of Smith (1971). Despite quantitative disagreement, there is qualitative agreement between measured and predicted values. The condensation and nucleation wave fronts are all concave with respect to the

https://doi.org/10.1017/S0022112097008379 Published online by Cambridge University Press

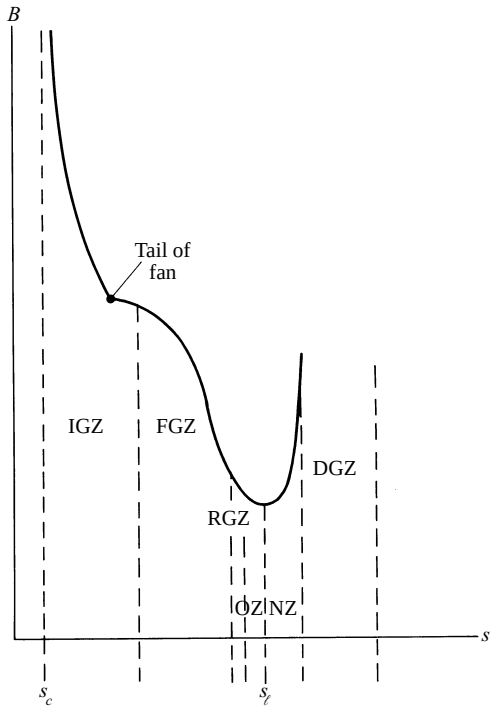


FIGURE 4. Typical variation of the normalized activation function B and the condensation zones along a streamline in the experiments of Smith (1971) (s_c is the streamwise location where saturation is reached and s_ℓ is the turning point of B).

oncoming flow. Also, as the relative humidity in the nozzle supply is increased, both the condensation and nucleation wave fronts move upstream in the expansion, as expected. However, the theoretical nucleation wave fronts are significantly delayed compared to the corresponding measured condensation wave fronts. In order to understand these differences, we proceed further to the heat addition zones using the algorithm developed for subcritical flows. Figure 6 shows the positions of two neighbouring expansion waves (Mach waves) in the (x', y')-plane for the expansion of moist air under the conditions of nozzle supply temperature $T_0' = 284$ K, specific humidity $w_0 = 6.8$ g kg^{-1} and relative humidity $\varphi_0 = 0.41$ in the experiments of Smith. As the nucleation wave front DF is traversed, the characteristics are curved toward the oncoming flow, showing clearly the effect of heat addition by condensation. Two typical neighbouring characteristics with initial inclination angles $\psi_{OM} = 39°$ and $\psi_{OD} = 30°$ are, respectively, shown by the curves OMP and ODQ. Even for this case, with the lowest available nozzle supply relative humidity at which measurements were carried out, the characteristics OMP and ODQ intersect, showing clearly the existence of an embedded shock wave for the conditions considered. This embedded shock wave pushes the nucleation wave front upstream towards a better agreement with the measured condensation wave front and is responsible for at least some of the quantitative differences mentioned above.

The predicted subcritical flow characteristics under the same nozzle supply conditions in the experiments of Smith along a typical streamline at a distance $D' = 9.86$ cm away from the corner at the nozzle throat are plotted in figures 7 and 8. The results show that the flow field in the nearly frozen zones is almost isentropic except

https://doi.org/10.1017/S0022112097008379 Published online by Cambridge University Press

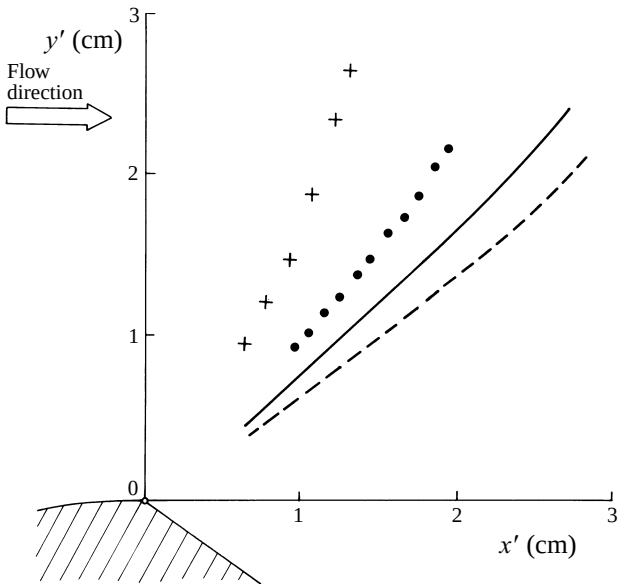


FIGURE 5. The measured onset conditions and the position of the subcritical nucleation wave front for the experiments of Smith (1971): •, measured onset conditions under nozzle supply temperature $T_0' = 284$ K, supply specific humidity $w_0 = 6.8$ g/kg and supply relative humidity $\varphi_0 = 0.41$; – – –, the corresponding nucleation wave front computed by the subcritical asymptotic solution. +, Measured onset conditions under nozzle supply temperature $T_0' = 284$ K, supply specific humidity $w_0 = 6.4$ g/kg and supply relative humidity $\varphi_0 = 0.69$; ———, the corresponding nucleation wave front computed by the subcritical asymptotic solution.

for the thin onset zone (OZ) where deviations from the isentropic solution begin to occur. It is important to realize that the subcritical solution thus obtained will be interrupted by the presence of an embedded shock wave due to excessive heat release by condensation as required by the intersecting characteristics in figure 6. The discussion of the origin and location of this embedded shock wave in the (x', y')-plane of figure 6 requires separate consideration and will not be considered here.

6. Conclusions

An asymptotic solution for corner expansion flows with homogeneous condensation has been presented for subcritical flows, i.e. flows not exceeding a critical amount of heat release by condensation. Distinct condensation zones with detailed analytical structure are exhibited along streamlines by the asymptotic solution of the condensation rate equation in the limit of a relatively slow nucleation process followed by rapid droplet growth. In particular the nucleation wave front, which corresponds to states of maximum nucleation, is constructed analytically independent of any nucleation and droplet growth models to be employed. The solution for the flow field along streamlines is given in closed form up to the location of the nucleation wave front and is seen to be almost isentropic, except within the thin onset zone (OZ). The flow field in the heat addition zones downstream of the nucleation wave front is also exhibited semi-analytically by the asymptotic solution for subcritical flows. Consequently an algorithm for the asymptotic solution of subcritical flows around a sharp corner can be constructed and rigorous computations under the experimental conditions reported by Smith (1971) can be carried out by this algorithm using the

https://doi.org/10.1017/S0022112097008379 Published online by Cambridge University Press

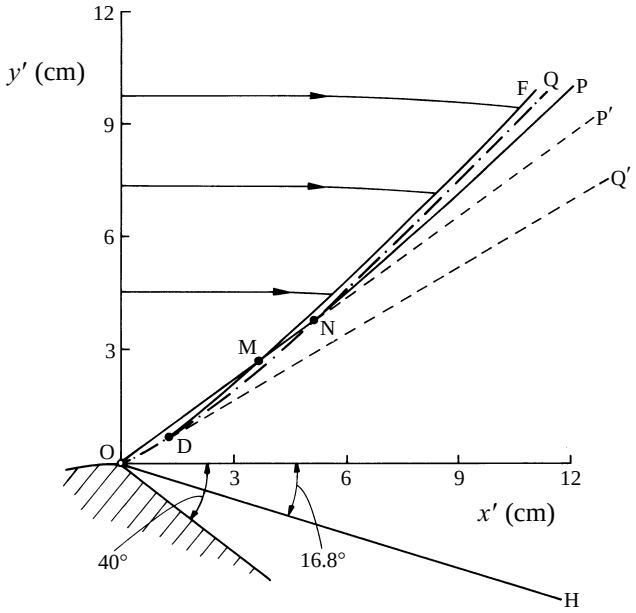


FIGURE 6. The characteristics, emanating from the corner and intersecting in the heat addition zones, computed by the subcritical asymptotic solution for the experiments of Smith (1971) under nozzle supply temperature $T_0' = 284$ K, supply specific humidity $w_0 = 6.8$ g kg^{-1} and supply relative humidity $\varphi_0 = 0.41$ (DF is the nucleation wave front, OMNP and ODNQ are, respectively, the characteristics with initial inclination angles $\psi_{OM} = 39°$ and $\psi_{OD} = 30°$ intersecting at point N, lines OMP′ and ODQ′ are the corresponding isentropic Mach lines).

classical nucleation theory and Hertz–Knudsen droplet growth law. In particular the onset measurements (condensation wave fronts) of Smith, with different initial relative humidities, are compared with the corresponding nucleation wave fronts obtained by this algorithm. Despite the experimental difficulties encountered in realizing Prandtl–Meyer flows around a sharp corner, some qualitative features can be established in comparing the results of Smith's (1971) experiments with those obtained by the subcritical algorithm:

(*a*) the nucleation and condensation wave fronts are both concave with respect to the oncoming flow;

(*b*) as the initial relative humidity is increased, the nucleation and condensation wave fronts both occur further upstream in the expansion fan;

(*c*) the flow field along streamlines is almost isentropic up to the nucleation wave front, except within the thin onset zone (OZ);

(*d*) the characteristics (or Mach lines) emerging from the corner, obtained by the semi-analytical asymptotic solution, are curved due to latent heat addition as they cross the nucleation wave front. Consequently the flow field within the heat addition zones deviates significantly from the self-similar solution of corner expansion flows.

However, the nucleation wave fronts obtained by the subcritical algorithm are considerably delayed compared to the onset measurements made by Smith (1971). Although some of the disagreement may result from the difficulties in realizing a Prandtl–Meyer expansion in the experiments of Smith, computations using the subcritical algorithm show intersecting characteristics in the heat addition zones, indicating the existence of an embedded oblique shock wave in the expansion fan

https://doi.org/10.1017/S0022112097008379 Published online by Cambridge University Press

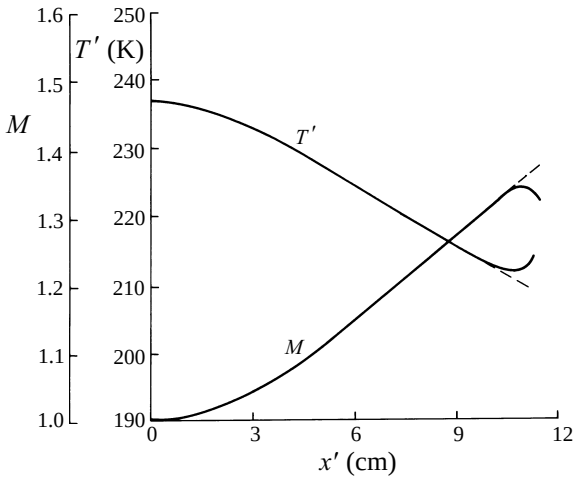


FIGURE 7. The distributions of the frozen Mach number M and temperature T' along a streamline with initial distance $D' = 9.86$ cm from the corner under the nozzle supply conditions stated in figure 6 for the experiments of Smith (1971) (dashed lines correspond to the isentropic solution).

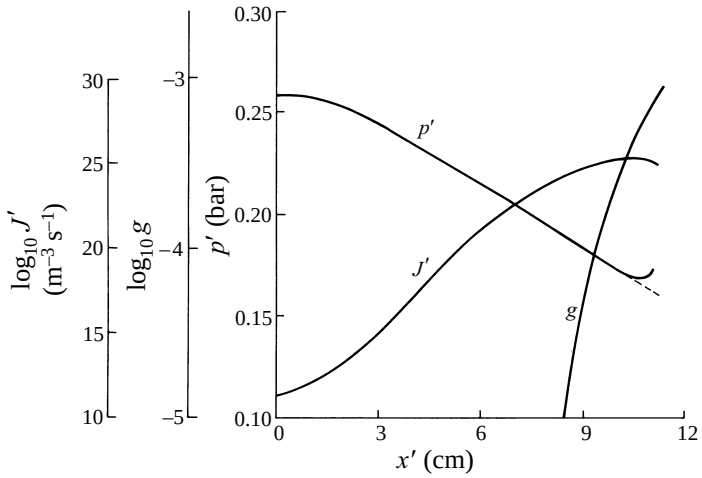


FIGURE 8. The distributions of the pressure p', the nucleation rate J' and the condensate mass fraction g along a streamline with initial distance $D' = 9.86$ cm from the corner under the nozzle supply conditions stated in figure 6 for the experiments of Smith (1971) (the dashed line corresponds to the isentropic pressure distribution).

(supercritical flows). This embedded oblique shock wave pushes the computed nucleation wave front upstream and seems to be responsible for most of the observed delay between the computed nucleation wave front and the measured onset conditions. The computation of the origin and location of this embedded shock together with the solution downstream of the shock requires separate consideration.

C. F. D. is grateful to the Royal Society and to the British Council for their support during his visit to the Department of Applied Mathematics and Theoretical Physics at the University of Cambridge. This work is also supported in part by the Scientific and Technical Research Council of Turkey (TÜBİTAK) and by the Turkish Academy of Sciences (TÜBA).

https://doi.org/10.1017/S0022112097008379 Published online by Cambridge University Press

REFERENCES

Abramowitz, M. & Stegun, A. 1965 *Handbook of Mathematical Functions*. Dover.

Barschdorff, D. 1971 Verlauf der Zustandsgrössen und gasdynamische Zusammenhänge bei der spontanen Kondensation reinen Wasserdampfes in Lavaldüsen. *Forsch. Ing. Wesen.* **37**, 146–156.

Barschdorff, D. 1975 Carrier gas effects on homogeneous nucleation of water vapor in a shock tube. *Phys. Fluids* **18**, 529–535.

Bartlmä, F. 1964 *Proc. 11th Intl Congress Appl. Mech., Munich.*

Blythe, P. A. & Shih, C. J. 1976 Condensation shocks in nozzle flows. *J. Fluid Mech.* **76**, 593–621.

Bratos, M. & Jaeschke, M. 1974 Two-dimensional flows with nonequilibrium phase transitions. *Inst. Podstawowych Problemow Tech. PAN, Warszawa* No. 58.

Clarke, J. H. & Delale, C. F. 1986 Nozzle flows with nonequilibrium condensation. *Phys. Fluids* **29**, 1398–1413.

Clarke, J. H. & Delale, C. F. 1988 Expansion flows on walls with nonequilibrium condensation. *Q. Appl. Maths* **46**, 121–143.

Courtney, W. G. 1965 Condensation in a rarefaction wave. *Tech. Rep.* 2, ONR NR 092517/4-29-65. Tiokol Chemical Corp., Denville, New Jersey.

Davydov, L. M. 1971 Study of nonequilibrium condensation in supersonic nozzles and jets. *Mech. Zhyid. Gaza* **3**, 66 (English transl. *Fluid Mech., Soviet Res.* 1972, **1**, 90).

Delale, C. F., Schnerr, G. H. & Zierep, J. 1993*a* Asymptotic solution of transonic nozzle flows with homogeneous condensation. I. Subcritical flows. *Phys. Fluids* A **5**, 2969–2981.

Delale, C. F., Schnerr, G. H. & Zierep, J. 1993*b* Asymptotic solution of transonic nozzle flows with homogeneous condensation. II. Supercritical flows. *Phys. Fluids* A **5**, 2982–2995.

Delale, C. F., Schnerr, G. H. & Zierep, J. 1995 Asymptotic solution of shock tube flows with homogeneous condensation. *J. Fluid Mech.* **287**, 93–118.

Erdelyi, A. 1956 *Asymptotic Expansions*, p. 36. Dover.

Frank, W. 1979 Prandtl–Meyer Expansion mit Wärmezufuhr. *Z. Angew. Math. Mech.* **59**, 223–226.

Frank, W. 1985 Condensation phenomena in supersonic nozzles. *Acta Mechanica* **54**, 135–156.

Gradshteyn, I. S. & Ryzhik, I. M. 1980 *Tables of Integrals, Series and Products*. Academic.

Gyarmathy, G. 1976 Thèorie de la condensation en cours de dètente dans les turbines à vapeur. *Rev. Française de Mèc.* **57**, 35–48.

Hill, P. G. 1966 Condensation of water vapor during supersonic expansion in nozzles. *J. Fluid Mech.* **25**, 593–620.

Homer, J. B. 1971 Studies on nucleation and growth of metallic particles from supersaturated vapors. *Shock Tube Research, Proc. Eighth Intl Shock Tube Symp., London* (ed. J. L. Stollery, A. G. Gaydon & P. R. Owen). Chapman and Hall.

Kalra, S. P. 1975 Experiments on nonequilibrium, nonstationary expansion of water vapor/carrier gas mixture in a shock tube. *University of Toronto, Institute of Aerospace Studies, Rep.* 195.

Kawada, H. & Mori, Y. 1973 A shock tube study on condensation kinetics. *Bull. JSME* **16**, 1053–1066.

Kotake, S. & Glass, I. I. 1981 Flows with nucleation and condensation. *Prog. Aerospace Sci.* **19**, 129–196.

Kurshakov, A. V., Saltanov, G. A. & Tkalenko, R. A. 1971 Theoretical and experimental investigation of condensation in a centered rarefaction wave. *Prikl. Mech. Tekn. Phys.* **5**, 117.

Oswatitsch, K. 1942 Kondensationerscheinung in Überschalldüsen. *Z. Angew. Math. Mech.* **22**, 1–14.

Peters, F. 1987 Condensation of supersaturated water vapor at low temperatures in a shock tube. *J. Phys. Chem.* **91**, 2487–2489.

Peters, F. & Paikert, B. 1989 Nucleation and growth rates of homogeneously condensing water vapor in argon from shock tube experiments. *Exps. Fluids* **7**, 521–530.

Schnerr, G. 1989 2-D transonic flow with energy supply by homogeneous condensation: Onset condition and 2-D structure of steady Laval nozzle flow. *Exps. Fluids* **7**, 145–156.

Schnerr, G. H. & Dohrmann, U. 1990 Transonic flow around airfoils with relaxation and energy supply by homogeneous condensation. *AIAA J.* **89**, 1187–1193.

Sirovich, L. 1971 *Techniques of Asymptotic Analysis*, p. 80. Springer.

Sislian, J. P. & Glass, I. I. 1976 Condensation of water vapor in rarefaction waves. I. Homogeneous nucleation. *AIAA J.* **14**, 1731–1737.

https://doi.org/10.1017/S0022112097008379 Published online by Cambridge University Press

Smith, L. T. 1971 Experimental investigation of the expansion of moist air around a sharp corner. *AIAA J.* **9**, 2035–2037.

Smolders, H. J., Niessen, E. M. J. & Dongen, M. E. H. van 1992 The random choice method applied to nonlinear wave propagation in gas-vapor-droplets mixtures. *Computers Fluids* **21**, 63–75.

Tkalenko, R. A. 1972 Condensation of water vapor during expansion in plane and axisymmetric nozzles. *Izv. Akad. Nauk SSSR, Mech. Zhyid. Gasa* **6**, 160.

Vincenti, G. W. & Kruger, C. H. 1965 *Introduction to Physical Gas Dynamics*. Wiley.

Wegener, P. P. 1969 Gasdynamics of expansion flows with condensation and homogeneous nucleation of water vapor. *In Nonequilibrium Flows* (ed. P. P. Wegener), Vol. 1, Part 1, p. 163. Marcel Dekker.

Wegener, P. P. & Mack, L. M. 1958 Condensation in supersonic and hypersonic wind tunnels. *Adv. Appl. Mech.* **5**, 307–447.

Wegener, P. P. & Pouring, A. A. 1964 Experiments on condensation of water vapor by homogeneous nucleation in nozzles. *Phys. Fluids* **7**, 352–361.

https://doi.org/10.1017/S0022112097008379 Published online by Cambridge University Press